within 1.6% by measurement [10]. These verify the accuracy of the large-signal FET FDTD modeling algorithm presented in this paper.

V. Conclusion

In this paper, a general algorithm for including large-signal active three-terminal models into the FDTD method is presented. A dynamic interface between the active device and the FDTD lattice is used to simulate the prominent nonlinear time-dependant behavior of the three-terminal active device, which is connected across multiple FDTD cells. A technique for introducing an internal EM-field absorber into the FDTD three-terminal active-device model in order to eliminate undesired current coupling is discussed. Numerical comparison shows this method is accurate and is expected to have general utility for other complicated hybrid lumped-circuit FDTD modeling situations.

Acknowledgment

The authors would like to thank Dr. A. D. Patterson and Dr. J. G. Leckey for valuable suggestions and fruitful discussions on FET modeling.

References

[1] W. Sui, D. A. Christensen, and C. H. Durney, "Extending the two-dimensional FDTD method to hybrid electromagnetic systems with active and passive lumped elements," *IEEE Trans. Microwave Theory Tech.*, vol. 40, pp. 724–730, Apr. 1992.

[2] V. A. Thomas, K. Ling, M. E. Jones, B. Toland, J. Lin, and T. Itoh, "FDTD analysis of an active antenna," *IEEE Microwave Guided Wave Lett.*, vol. 4, pp. 296–298, Sept. 1994.

[3] C. Kuo, S. T. Chew, B. Houshmand, and T. Itoh, "FDTD simulation of a microwave amplifier," in *Int. IEEE MTT-S Dig.*, Orlando, FL, May 1995, pp. 357–360.

[4] P. Ciampolini, P. Mezzanotte, L. Roselli, D. Sereni, R. Sorrentino, and P. Torti, "Simulation of HF circuits with FDTD technique including nonlinear lumped elements," in *Int. IEEE MTT-S Dig.*, Orlando, FL, May 1995, pp. 361–364.

[5] C. H. Durney, W. Sui, D. A. Christensen, and J. Zhu, "A general formulation for connecting sources and passive lumped-circuit elements across multiple 3-D FDTD cells," *IEEE Microwave Guided Wave Lett.*, vol. 6, pp. 85–87, Feb. 1996.

[6] M. Piket-May, A. Taflove, and J. Baron, "FD-TD modeling of digital signal propagation in 3-D circuits with passive and active loads," *IEEE Trans. Microwave Theory Tech.*, vol. 42, pp. 1514–1523, Aug. 1994.

[7] Q. Chen and V. F. Fusco, "A new algorithm for analysing lumped parameter elements using 3D FDTD method," in *25th European Microwave Conf. Proc.*, Bologna, Italy, Sept. 1995, pp. 410–413.

[8] R. S. Pengelly, *Microwave Field-Effect Transistors—Theory, Design and Applications*. New York: Wiley, 1986, ch. 8.

[9] Q. Chen and V. F. Fusco, "Three-dimensional finite-difference time-domain slotline analysis on a limited memory personal computer," *IEEE Trans. Microwave Theory Tech.*, vol. 43, pp. 358–362, Feb. 1995.

[10] ____, "Time-domain diakoptics active slot-ring antenna analysis using FDTD," in *Proc. 26th European Microwave Conf.*, Prague, Czech Republic, Sept. 1996, pp. 440–443.

Resonance in a Cylindrical–Triangular Microstrip Structure

Kin-Lu Wong and Shan-Cheng Pan

***Abstract*—Full-wave solutions for the complex-resonant frequency of a triangular microstrip patch printed on a cylindrical substrate are presented. Curvature effects on the complex-resonant frequency, as well as the quality factor of the cylindrical–triangular microstrip structure, are analyzed. Measured resonant frequencies are also shown for comparison. Good agreement between measured and theoretical results is obtained.**

***Index Terms*—Microstrip antenna, microstrip resonator.**

I. Introduction

Characteristics of triangular microstrip structures used as resonators [1] or radiators [2], [3] have been reported. Results have shown that, as a resonator, the triangular microstrip structure at its fundamental mode (TM_{10} [1]) has a lower radiation loss than the circular microstrip resonators. It is also reported that, compared to the rectangular microstrip patch antenna, the microstrip antenna with a triangular patch is physically smaller and has similar radiation properties [2]. It is also noted that the related studies are mainly of planar geometries, and very scant results for the triangular microstrip patch mounted on a cylindrical substrate are available. This kind of cylindrical microstrip structure has the advantage of conformability and can find applications on curved surfaces such as those of aircraft and missiles.

In this paper, the theoretical analysis of the cylindrical–triangular microstrip structure is performed using a full-wave formulation. A basis function similar to the true current distribution on the patch surface is also selected for efficient and accurate numerical calculation. Numerical results for the complex-resonant frequencies [4], [5] of the microstrip structure are presented and discussed, and the quality factor of the microstrip structure is also analyzed. Measured resonant frequencies are also shown for comparison.

II. Theoretical Formulation

Fig. 1 shows the geometry of a cylindrical–triangular microstrip structure. The radius of the ground cylinder is a, and the cylindrical substrate has a thickness of h and a relative permittivity of ε_r. The sidelength of the triangular patch in the ϕ direction is d_2 $(= 2b\phi_0)$, and the other two sides are assumed to have the same length of d_1. The relationship of d_1 and d_2 is given by

$$d_1 = \sqrt{(d_2/2)^2 + (2z_0)^2} \tag{1}$$

where $2z_0$ is the distance from the tip of the triangle to the bottom side of the triangle.

To begin with, the full-wave formulation in [4] is followed, and the following equation is obtained:

$$\begin{bmatrix} \tilde{E}_\phi(n,k_z) \\ \tilde{E}_z(n,k_z) \end{bmatrix} = \overline{\overline{Q}}(n,k_z) \cdot \begin{bmatrix} \tilde{J}_\phi(n,k_z) \\ \tilde{J}_z(n,k_z) \end{bmatrix} \tag{2}$$

Manuscript received November 5, 1996; revised March 17, 1997. This work was supported by the National Science Council of the Republic of China under Grant NSC85-2221-E-110-002.

The authors are with the Department of Electrical Engineering, National Sun Yat-Sen University, Kaohsiung, Taiwan 804, R.O.C.

Publisher Item Identifier S 0018-9480(97)05387-8.

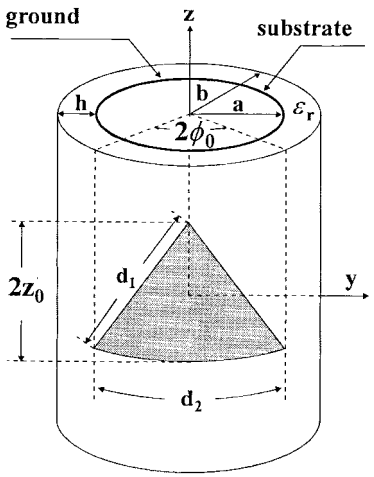

Fig. 1. The geometry of a cylindrical–triangular microstrip structure.

where E_ϕ and E_z are the tangential components of the electric field at $\rho = b$, and J_ϕ and J_z are the tangential components of the patch surface-current density; $\bar{\bar{Q}} = \hat{\phi}Q_{\phi\phi}\hat{\phi} + \hat{\phi}Q_{\phi z}\hat{z} + \hat{z}Q_{z\phi}\hat{\phi} + \hat{z}Q_{zz}\hat{z}$ is the dyadic Green's function, whose expressions have been derived and interpreted in [4]. The tilde in the equation denotes a Fourier transform.

Next, to solve the unknown patch surface current, a basis function is selected, which satisfies the criterion that the normal component of the electric surface-current density should vanish at the patch edges [2]. This selected basis function for the fundamental mode (TM_{10}) excitation is expressed as

$$J_\phi(\phi, z) = \frac{b\phi}{z - z_0}\sin\left[\frac{(z + z_0)\pi}{2z_0}\right] \tag{3}$$

$$J_z(\phi, z) = \sin\left[\frac{(z + z_0)\pi}{2z_0}\right]. \tag{4}$$

In this case, the unknown patch surface-current density can be written as

$$J(\phi, z) = I_\phi J_\phi(\phi, z) + I_z J_z(\phi, z) \tag{5}$$

where I_ϕ and I_z are unknown coefficients to be determined. It should be noted that since the next higher order mode (TM_{11}) has a resonant frequency about 1.73 times that of the fundamental TM_{10} mode [1], the effects of the TM_{11} mode and other higher order modes on the characteristics of the TM_{10} mode can be ignored. Thus, it is appropriate to use only one basis function to simulate the excited patch surface-current density for the TM_{10} mode. Then, by taking the spectral amplitude of the selected basis function, imposing the boundary condition that the patch surface current and the electric field are complementary to each other at $\rho = b$, and using the selected basis function as the testing function and integrating it over the patch area, one has [4]

$$\begin{bmatrix} Z_{\phi\phi} & Z_{\phi z} \\ Z_{z\phi} & Z_{zz} \end{bmatrix}\begin{bmatrix} I_\phi \\ I_z \end{bmatrix} = \begin{bmatrix} 0 \\ 0 \end{bmatrix} \tag{6}$$

where

$$Z_{\phi\phi} = \sum_{n=-\infty}^{\infty}\int_{-\infty}^{\infty} dk_z \tilde{J}_\phi(-n, -k_z)Q_{\phi\phi}\tilde{J}_\phi(n, k_z) \tag{7}$$

$$Z_{\phi z} = \sum_{n=-\infty}^{\infty}\int_{-\infty}^{\infty} dk_z \tilde{J}_\phi(-n, -k_z)Q_{\phi z}\tilde{J}_z(n, k_z) \tag{8}$$

$$Z_{z\phi} = \sum_{n=-\infty}^{\infty}\int_{-\infty}^{\infty} dk_z \tilde{J}_z(-n, -k_z)Q_{z\phi}\tilde{J}_\phi(n, k_z) \tag{9}$$

$$Z_{zz} = \sum_{n=-\infty}^{\infty}\int_{-\infty}^{\infty} dk_z \tilde{J}_z(-n, -k_z)Q_{zz}\tilde{J}_z(n, k_z) \tag{10}$$

with

$$\tilde{J}_\phi(n, k_z) = \frac{-j}{2\pi}\int_{-z_0}^{z_0} dz e^{-jk_z z} \times \left\{\frac{-\phi_0}{nz_0}\sin\left[\frac{\pi}{2z_0}(z + z_0)\right]\cos\left[\frac{n\phi_0}{2z_0}(z - z_0)\right] + \frac{2}{n^2(z - z_0)}\sin\left[\frac{n\phi_0}{2z_0}(z - z_0)\right]\right\}. \tag{11}$$

For $n \neq 0$

$$\tilde{J}_z(n, k_z) = \frac{-1}{2nz_0}\left\{\sin\frac{n\phi_0}{2}\left[\frac{\cos\left(k_z + \frac{n\phi_0}{2z_0}\right)z_0}{\left(k_z + \frac{n\phi_0}{2z_0}\right)^2 - \left(\frac{\pi}{2z_0}\right)^2} + \frac{\cos\left(k_z - \frac{n\phi_0}{2z_0}\right)z_0}{\left(k_z - \frac{n\phi_0}{2z_0}\right)^2 - \left(\frac{\pi}{2z_0}\right)^2}\right] - j\cos\frac{n\phi_0}{2}\left[\frac{\cos\left(k_z + \frac{n\phi_0}{2z_0}\right)z_0}{\left(k_z + \frac{n\phi_0}{2z_0}\right)^2 - \left(\frac{\pi}{2z_0}\right)^2} + \frac{\cos\left(k_z - \frac{n\phi_0}{2z_0}\right)z_0}{\left(k_z - \frac{n\phi_0}{2z_0}\right)^2 - \left(\frac{\pi}{2z_0}\right)^2}\right]\right\} \tag{12a}$$

and for $n = 0$

$$\tilde{J}_z(n, k_z) = \frac{-\phi_0}{2\pi z_0}\left\{\frac{j2}{\left(\frac{\pi}{2z_0}\right)^2 - k_z^2}\left[\frac{k_z\pi\cos k_z z_0}{z_0\left[\left(\frac{\pi}{2z_0}\right)^2 - k_z^2\right]} - \frac{\pi\sin k_z z_0}{2}\right] - \frac{\pi\cos k_z z_0}{\left(\frac{\pi}{2z_0}\right)^2 - k_z^2}\right\}. \tag{12b}$$

To have nontrivial solutions for I_ϕ and I_z in (6), it is required that

$$\det\begin{bmatrix} Z_{\phi\phi} & Z_{\phi z} \\ Z_{z\phi} & Z_{zz} \end{bmatrix} = 0. \tag{13}$$

By solving (13), a solution is obtained for the complex frequency $f = f' + jf''$, where f' and f'' are, respectively, the resonant frequency and radiation loss of the microstrip structure, and $f'/2f''$ is the quality factor of the microstrip structure.

III. Results and Discussion

The calculated complex-resonant frequencies of the cylindrical–triangular microstrip structure at the fundamental mode are presented. Fig. 2 shows the results for an equilateral-triangular microstrip patch with a sidelength of 5.78 cm mounted on ground cylinders having $a = 7.8$, 15, and 20 cm. Measured data for the resonant frequencies of the triangular patch printed on a substrate of thickness $h = 0.762$ mm and relative permittivity $\varepsilon_r = 3.0$ are also shown for comparison. Good agreement between the measured and calculated results is obtained. From the results, it is seen that the resonant frequency (real part of the complex-resonant frequency) increases with decreasing cylinder radius. This behavior is probably due to the decrease in the effective patch size, which occurs when the microstrip patch is mounted on a ground cylinder of smaller radius. As for the imaginary part of the complex-resonant frequency, it is seen that it increases with increasing curvature. This implies that the radiation loss of the microstrip structure increases when the cylindrical–triangular patch has a smaller cylinder radius. This observation is similar to those made in the cases of cylindrical–rectangular microstrip structures [4] and spherical–circular microstrip structures [5]. From the complex-resonant frequency results, the quality factor of the microstrip

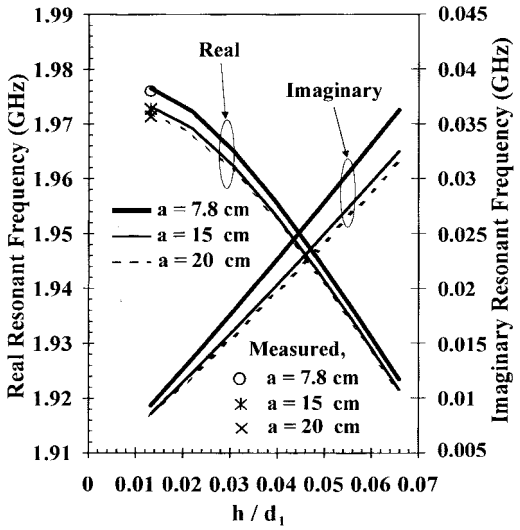

Fig. 2. Real and imaginary parts of complex-resonant frequency versus normalized substrate thickness for different cylinder radii of $a = 7.8$, 15, 20 cm; $\varepsilon_r = 3.0$, $d_1 = d_2 = 5.78$ cm.

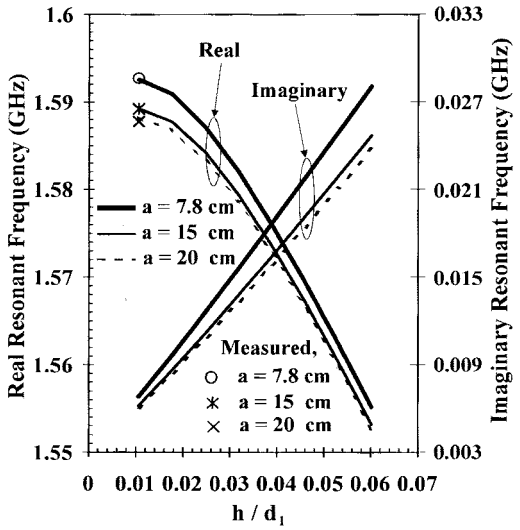

Fig. 4. Real and imaginary parts of complex-resonant frequency versus normalized substrate thickness for different cylinder radii of $a = 7.8$, 15, 20 cm; $\varepsilon_r = 3.0$, $d_1 = d_2 = 7.18$ cm.

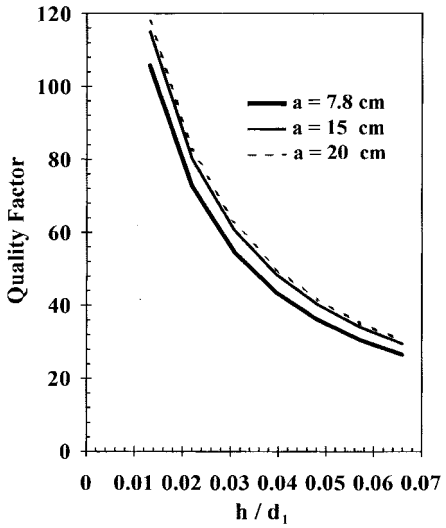

Fig. 3. Quality factor versus normalized substrate thickness for the case shown in Fig. 2.

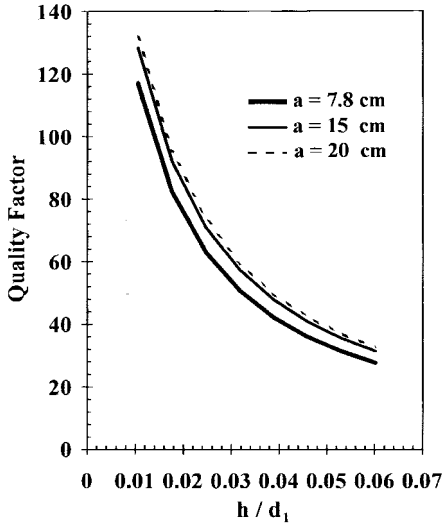

Fig. 5. Quality factor versus normalized substrate thickness for the case shown in Fig. 4.

structure can be readily calculated, and is presented in Fig. 4. It is seen that the quality factor decreases with decreasing cylinder radius. This suggests that a planar–triangular microstrip structure is more suitable for use as a resonator than a cylindrical–triangular microstrip structure.

Another case of the equilateral triangular patch with a sidelength of 7.18 cm was also studied. Results are presented in Figs. 4 and 5. Behavior similar to that shown in Figs. 2 and 3 is also observed. The measured resonant frequencies are also in good agreement with the calculated results.

IV. Conclusion

The complex-resonant frequencies of a cylindrical–triangular microstrip structure have been studied using a full-wave approach. By selecting a suitable basis function, which satisfies the requirement that the patch surface current vanishes at the patch edges, the calculated resonant frequencies are found to agree well with the measured data. The observed curvature effects on the characteristics of cylindrical–triangular microstrip structures excited at the fundamental mode are also found to be similar to those reported for rectangular microstrip patches printed on a cylindrical substrate [4] or circular microstrip patches printed on a spherical substrate [5].

References

[1] J. Helszajn and D. S. James, "Planar triangular resonators with magnetic walls," *IEEE Trans. Microwave Theory Tech.*, vol. MTT-26, pp. 95–100, Feb. 1978.

[2] H. R. Hassani and D. Mirshekar, "Analysis of triangular patch antennas including radome effects," *Proc. Inst. Elect. Eng.*, pt. H, vol. 139, pp. 251–256, June 1992.

[3] K. F. Lee, K. M. Luk, and J. S. Dahele, "Characteristics of the equilateral triangular patch antenna," *IEEE Trans. Antennas Propagat.*, vol. 36, pp. 1510–1518, Nov. 1988.

[4] K. L. Wong, Y. T. Cheng, and J. S. Row, "Resonance in a superstrate-loaded cylindrical-rectangular microstrip structure," *IEEE Trans. Microwave Theory Tech.*, vol. 41, pp. 814–819, May 1993.

[5] K. L. Wong and H. T. Chen, "Resonance in a spherical-circular microstrip structure with an airgap," *IEEE Trans. Microwave Theory Tech.*, vol. 41, pp. 1446–1468, Aug. 1993.